NUREG/CR-2647
ANL-82-6

NUREG/CR-2647
ANL-82-6

CRITICAL HEAT-FLUX EXPERIMENTS UNDER LOW-FLOW CONDITIONS IN A VERTICAL ANNULUS

by

K. Mishima and M. Ishii

ARGONNE NATIONAL LABORATORY

ARGONNE NATIONAL LABORATORY, ARGONNE, ILLINOIS

Prepared for the Office of Nuclear Regulatory Research
U. S. NUCLEAR REGULATORY COMMISSION
under Interagency Agreement DOE 40-550-75

DISCLAIMER

The facilities of Argonne National Laboratory are owned by the United States Government. Under the terms of a contract (W-31-109-Eng-38) among the U. S. Department of Energy, Argonne Universities Association and The University of Chicago, the University employs the staff and operates the Laboratory in accordance with policies and programs formulated, approved and reviewed by the Association.

MEMBERS OF ARGONNE UNIVERSITIES ASSOCIATION

The University of Arizona
Carnegie-Mellon University
Case Western Reserve University
The University of Chicago
University of Cincinnati
Illinois Institute of Technology
University of Illinois
Indiana University
The University of Iowa
Iowa State University
The University of Kansas
Kansas State University
Loyola University of Chicago
Marquette University
The University of Michigan
Michigan State University
University of Minnesota
University of Missouri
Northwestern University
University of Notre Dame
The Ohio State University
Ohio University
The Pennsylvania State University
Purdue University
Saint Louis University
Southern Illinois University
The University of Texas at Austin
Washington University
Wayne State University
The University of Wisconsin-Madison

Available from

GPO Sales Program
Division of Technical Information and Document Control
U. S. Nuclear Regulatory Commission
Washington, D.C. 20555

and

National Technical Information Service
Springfield, Virginia 22161

NUREG/CR-2647
ANL-82-6
(Distribution Codes: R2 and R4)

ARGONNE NATIONAL LABORATORY
9700 South Cass Avenue
Argonne, Illinois 60439

NUREG/CR--2647

DE82 009965

CRITICAL HEAT-FLUX EXPERIMENTS UNDER LOW-FLOW CONDITIONS IN A VERTICAL ANNULUS

by

K. Mishima* and M. Ishii

Reactor Analysis and Safety Division

March 1982

Prepared for the Division of Accident Evaluation
Office of Nuclear Regulatory Research
U. S. Nuclear Regulatory Commission
Washington, D. C. 20555
Under Interagency Agreement DOE 40-550-75

NRC FIN No. A2026

*Now at Research Reactor Institute, Kyoto University, Kyoto, Japan

CRITICAL HEAT FLUX EXPERIMENTS UNDER LOW FLOW CONDITIONS IN A VERTICAL ANNULUS

by

K. Mishima and M. Ishii

ABSTRACT

An experimental study was performed on critical heat flux (CHF) at low flow conditions for low pressure steam-water upward flow in an annulus. The test section was transparent, therefore, visual observations of dryout as well as various instrumentations were made. The data indicated that a premature CHF occurred due to flow regime transition from churn-turbulent to annular flow. It is shown that the critical heat flux observed in the experiment is essentially similar to a flooding-limited burnout and the critical heat flux can be well reproduced by a nondimensional correlation derived from the previously obtained criterion for flow regime transition. The observed CHF values are much smaller than the standard high quality CHF criteria at low flow, corresponding to the annular flow film dryout. This result is very significant, because the coolability of a heater surface at low flow rates can be drastically reduced by the occurrence of this mode of CHF.

NRC FIN No.	Title
A2026	Phenomenological Modeling of Two-phase Flow in Water Reactor Safety

TABLE OF CONTENTS

LIST OF FIGURES

LIST OF TABLES

THIS PAGE

WAS INTENTIONALLY

LEFT BLANK

NOMENCLATURE

A	Flow area
A_h	Heated area
C	Constant which appears in the flooding correlation
C_o	Distribution parameter
D	Hydraulic diameter
D_h	Heated equivalent diameter
D^*	Non-dimensional hydraulic diameter defined by Eq. (15)
G	Mass velocity
G^*	Non-dimensional mass velocity defined by Eq. (14)
g	Gravity
h_{fg}	Latent heat of vaporization
J	Non-dimensional parameter defined by Eq. (19)
j	Volumetric flux of two-phase mixture = $j_g + j_f$
j_k	Volumetric flux of k phase
j_k^*	Non-dimensional volumetric flux of k phase
j_{gc}	Volumetric flux of vapor entering the heated section from the bottom as shown in Fig. 9
K	Constant
L	Heated length
N_μ	Viscosity number as defined by Eq. (54)
n	Constant
Q	Total heat input
q_c	Critical heat flux
q^*	Non-dimensional burnout heat flux defined by Eq. (13)
Re_f	Liquid Reynolds number defined by Eq. (55)
Z	Distance from the bottom in the flow direction
α	Void fraction
α_m	Mean void fraction in a slug bubble section
Δh_i	Inlet enthalpy subcooling of fluid
Δh_{BO}	Enthalpy subcooling at burnout location
$\Delta\rho$	Absolute value of density difference
ζ	Non-dimensional parameter defined by Eq. (29)
λ	Characteristic wave length of Taylor instability
μ_k	Viscosity of k phase
ν_k	Kinematic viscosity of k phase
ρ_k	Density of k phase
σ	Surface tension

Subscripts

f	Liquid phase
g	Gas or vapor phase

CRITICAL HEAT FLUX EXPERIMENTS UNDER LOW FLOW CONDITIONS IN A VERTICAL ANNULUS

by

K. Mishima and M. Ishii

ABSTRACT

An experimental study was performed on critical heat flux (CHF) at low flow conditions for low pressure steam-water upward flow in an annulus. The test section was transparent, therefore, visual observations of dryout as well as various instrumentations were made. The data indicated that a premature CHF occurred due to flow regime transition from churn-turbulent to annular flow. It is shown that the critical heat flux observed in the experiment is essentially similar to a flooding-limited burnout and the critical heat flux can be well reproduced by a nondimensional correlation derived from the previously obtained criterion for flow regime transition. The observed CHF values are much smaller than the standard high quality CHF criteria at low flow, corresponding to the annular flow film dryout. This result is very significant, because the coolability of a heater surface at low flow rates can be drastically reduced by the occurrence of this mode of CHF.

EXECUTIVE SUMMARY

The occurrences of burnout in natural convection boiling can be very important in relation to the safety of various types of nuclear reactors under a number of different accident conditions. It is noted that accidents which lead to the decay heat removal by natural circulation have much higher probability than those of the severe accidents extensively studied recently. However, the break-down of the natural circulation boiling which leads to dryout and burnout of heated surface in these conditions can have a very significant consequence.

In view of the above, an experimental study has been performed on the critical heat flux at low flow rates typical of natural circulation conditions. Data have been obtained for water from an annulus test section at low pressure. The data indicated that a premature burnout occurred due to flow regime transition from churn-turbulent to annular flow. It has been shown that the burnout observed in the experiment is similar to a flooding-limited burnout, although the loop circulation has been maintained at a near natural convection level. The data can be well correlated by the newly developed CHF criterion derived from the churn-turbulent to annular flow transition criterion.

Since the outer tube of the test section was a Pyrex glass tube, a detailed visual observation on the dryout and rewetting processes have been made. Dry patches appeared on the surface of the heated wall in the churn-turbulent flow regime. However, they were repeatedly rewetted mainly by the passages

of liquid slugs or bridges. In this experiment, permanent dryout of the heated wall occurred when these liquid bridges disappeared at the churn-turbulent to annular flow transition. Falling liquid film as well as climbing film was observed at this point, however, those liquid film did not seem thick enough to quench dry patches.

Due to the above mechanism of CHF, the observed critical heat flux values are much smaller than the standard pool boiling or high quality CHF criteria. There are some indications that the presently observed premature burnout may be limited to a low pressure system with relatively high inlet flow restrictions. However, at the present boundaries between different CHF mechanisms are not well established. Hence, finding of this new premature burnout mechanism is quite important. If this mode of CHF has to occur, the coolability of a heated surface at low flow rates can be drastically overpredicted by using the conventional high quality CHF criterion.

I. INTRODUCTION

Natural convection boiling burnout can become important in relation to the safety of various types of liquid cooled nuclear reactors under a number of different accident conditions such as loss-of-heat sink, loss-of-flow and loss-of-piping integrity accidents. In spite of the importance of the cooling due to natural convection boiling and its upper limitation imposed by occurrences of the burnout, the main emphases of reactor safety analyses both for water and liquid-metal cooled reactors have been directed to more drastic accident conditions where the natural convection boiling is of little importance. However, it can be recognized that milder accidents which lead to the decay heat removal by near natural circulation boiling have much higher probability than those severe accidents extensively studied recently. Furthermore, the break-down of the natural circulation boiling can lead to a very significant consequence as exemplified by the Three-Mile Island accident under the small LOCA (loss-of-coolant accident) condition.

A number of different accidents can lead to cooling of a reactor core by natural convection boiling. These are small LOCA's for light water reactors, loss-of-flow accidents due to pump failure with mismatched decay heat, loss-of-heat sink accidents both for light water and liquid-metal cooled reactors, and loss-of-piping integrity for loop type liquid-metal cooled reactors. Regardless of the initial stages of these accidents, a similar condition which is basically the decay heat removal by the natural convection boiling can develop. For example, in case of a pump failure, the reactor will be shut down or set back immediately to reduce the heat load. As the resistance of the flow channels forces the coolant to stagnate, a transition of coolant flow to natural convection will follow. During this period, some flow instability may occur[1] which may cause a premature burnout.[2] Eventually a stable natural convection may be attained. However, a burnout can occur before the decay heat becomes sufficiently low if the period of the flow coast down is too short. On the other hand, if the flow coast down lasts long enough, a natural convection will allow the core to be cooled safely without any additional cooling devices.

The purpose of this study is to provide an insight into burnout phenomena which can occur during natural convection boiling and to recommend a correlation of practical use to estimate the critical heat flux at such low flow rates as natural convection. As a first step, the critical heat flux for water in an annulus at about atmospheric pressure have been studied. Burnout at a stagnant flow condition was also included in this study as a limiting case of burnout phenomena.[3] An experiment has been carried out using the modified Freon Test Loop with an annular test section at Argonne National Laboratory.[4] From the experimental data and the review of previous works, nondimensional correlations are derived and discussed in detail.

II. CRITICAL HEAT FLUX EXPERIMENT

A. Test Loop

The test loop was initially set up for Freon-11 blowdown tests[4] and modified for this study as shown in Fig. 1. It consisted of test section, upper and lower plena, hot and cold legs, downcomer, bypass loop, circulating pump, flow control valves and turbine flowmeter. The test loop was thermally insulated by fiberglass material except the test section.

The test section is made of a 86 cm-long, 2.045 cm-OD, directly heated, Type 304 stainless steel tube and a 0.9 m-long, 2.5959 cm-ID transparent Pyrex pipe. Twenty-two 0.762 mm-OD, Chromel-Alumel thermocouples were spot-welded onto the inside wall of the stainless steel tube as shown in Fig. 2. The detail of the test section was already described in Ref. 4.

The downcomer consisted of a 180 cm-long, 15 cm-ID stainless steel tube flanged at both ends, equipped with a cooling coil of a 12 m-long, 3 mm-ID copper tube, a 5 kW immersion heater, a steam release valve and a water supply.

A 1.58 cm-ID stainless steel flexible tube was installed in the hot and the cold leg to allow a thermal expansion and to avoid the vibration of the test section induced by the pump during forced convection experiments. The cold leg consisted of two parallel flow paths, one for natural convection and the other for forced convection. A pump capable of delivering up to 0.5 ℓ/min of water was installed in the latter cold leg.

B. Experimental Procedure

Before starting the measurements, the water in the test loop was heated up with the immersion heater and the test section heater. During the heatup operation, the power to the test section was kept so low as not to cause dryout on the surface of the heated wall. Power to the test section was supplied by a 20-V, 1500-A, dc power supply. To protect the test section from physical burnout, nine temperature controllers were set to trip the power at a heated-wall temperature of 200°C. The detail of the controllers also appear in the literature.[4] The power to the test section was estimated by measuring the voltage drop across the test section and that across an on-line shunt rated at 50 mV/2000 A.

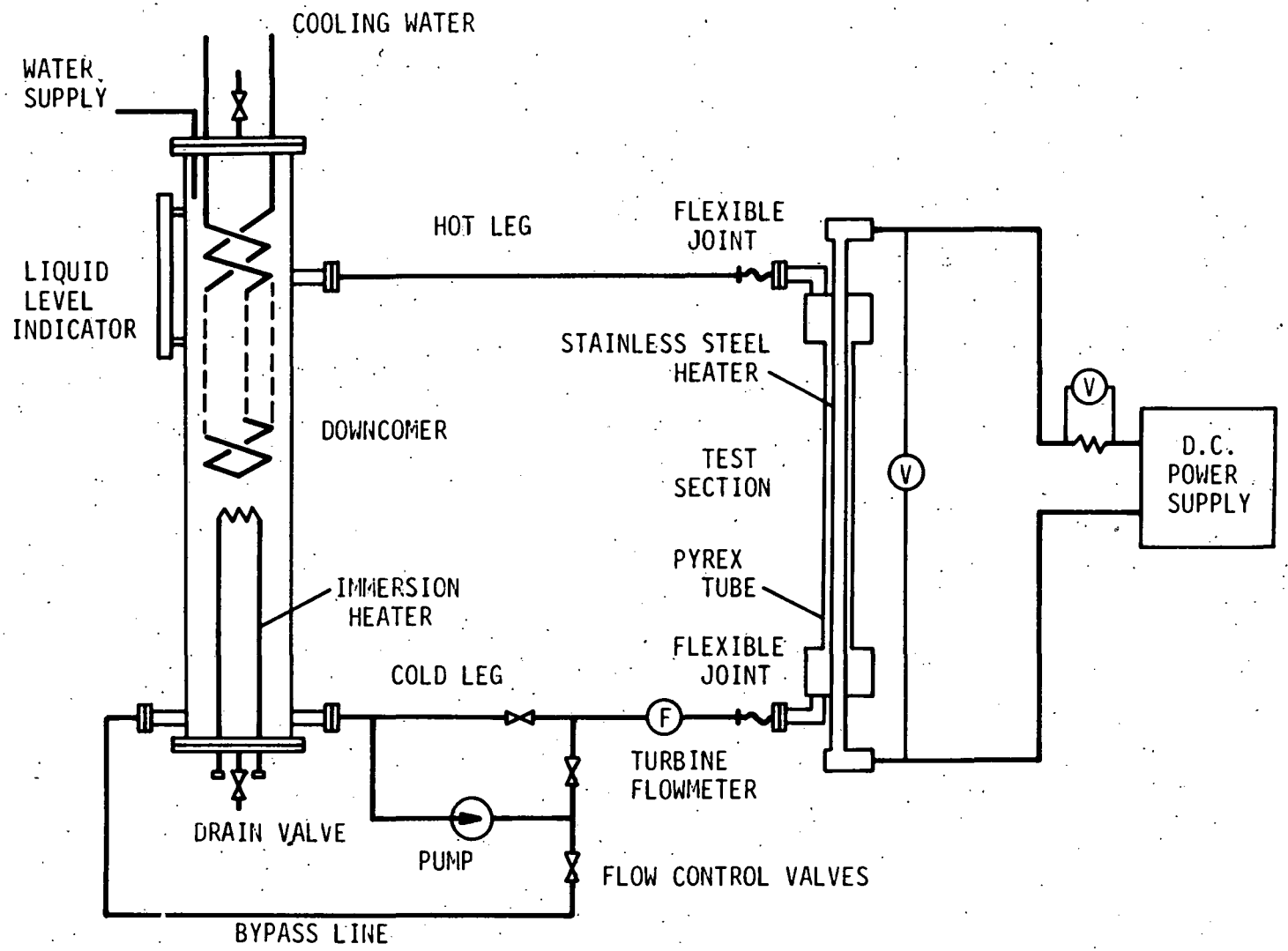

Fig. 1. Schematic Showing of the Test Rig

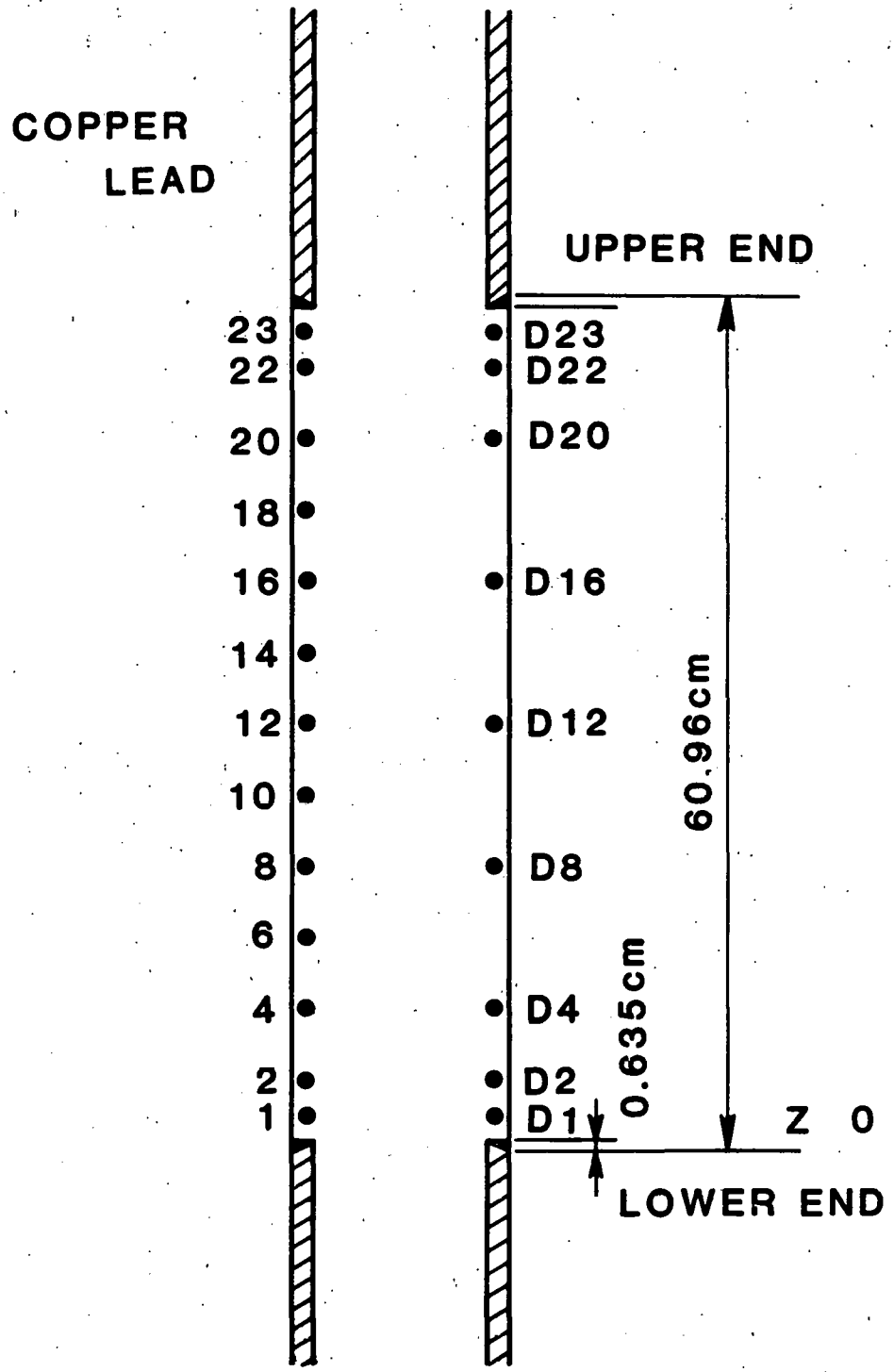

Fig. 2. Thermocouple Locations. The numbers denote the distance from Z = 0 measured in inch.

The loop was filled with ion-exchanged water to a level several centimeters above the hot leg which was observed in the glass tube attached to the downcomer. To avoid overpressure in the loop, the vent valve on top of the downcomer was left open during the experiment. Thus all the measurements were carried out under atmospheric pressure.

The water flow rate into the test section was controlled by the valves installed in the cold leg. Test condition covered natural convection, forced convection and zero net flow with the inlet valves fully closed. The water flow rate was measured by a turbine flowmeter (Cox Instrument, Model LF-6-00). The flowmeter was calibrated within 4%.

The temperatures were recorded by a digital recorder. As dry patches were more frequently observed on the surface near the upper end of the heated wall, the temperature at the location of TC 22 was recorded also by a Honeywell strip chart. A large abrupt increase in the temperature trace was recognized as an evidence of dryout as well as the actuation of the power trip circuit.

III. EXPERIMENTAL RESULTS

A. Flow Regimes

In order to observe flow regimes over a wide range of water flow rate, the flowmeter was replaced by a 1.58 cm-ID pipe in earlier runs, thus reducing the resistance to the flow. In these runs, the flow rate was estimated from the axial profile of the heated-wall temperature, assuming that the single phase heat transfer coefficient was constant over the non-boiling region. If this was true, the water flow rate should be proportional to the reciprocal of the temperature rise along the test section.

At an early stage of the heatup, the initiation of boiling occurred suddenly with a large slug bubble, followed by intermittent bubble formation. During this period, highly agitated inlet flow was observed as shown in Fig. 3. As the flow approached steady, smaller bubbles were generated more frequently, resulting in a more stable flow.

No significant difference in flow regimes between natural convection and forced convection was noticed in the test section. Observed flow regimes are shown in Fig. 4 compared with the flow regime map predicted by the authors.[5] Bubbly flow was scarcely observed at low heat flux and large inlet subcooling. Slug flow which appeared in the figure was characterized by the periodic slug bubble formation, though the shape of the bubble was disturbed by boiling. In the churn-turbulent flow, slug-like bubbles were entirely deformed and less periodic and liquid bridging was typically observed. Dry patches appeared on the surface of the heated wall in this flow regime, though they were quenched away mainly by the passage of liquid bridges. The temperature rise due to dry patch formation was found in the strip chart as shown in Fig. 5.

As the steam quality increased, the liquid bridging became less frequent. Falling liquid film as well as climbing film was observed at low mass velocities. Those liquid film, however, did not seem thick enough to quench dry patches, thus permanent dryout of the heated wall followed. A typical reading

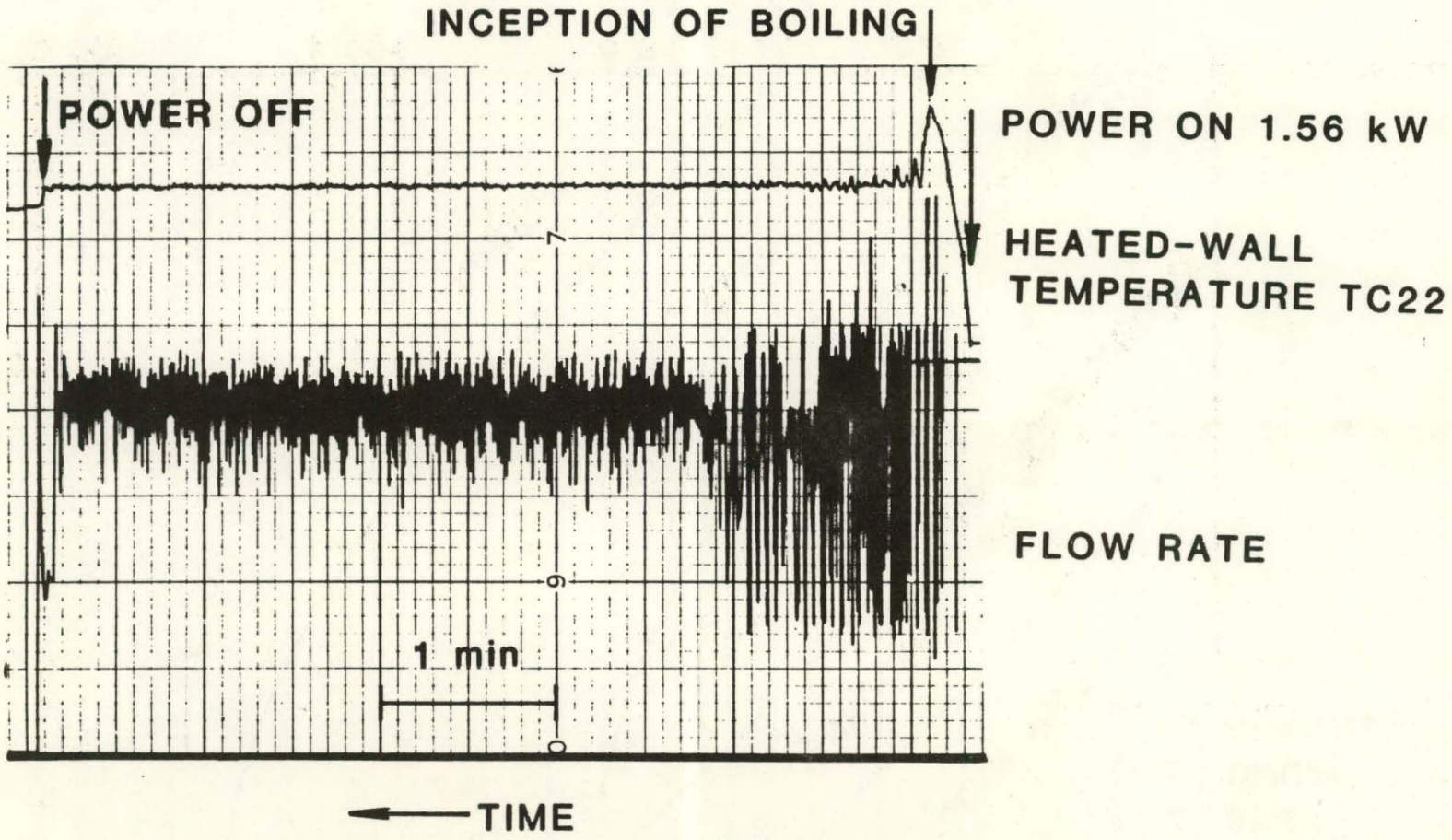

Fig. 3. Heated-wall Temperature and Flow Rate Traces at an Early Stage of Heatup

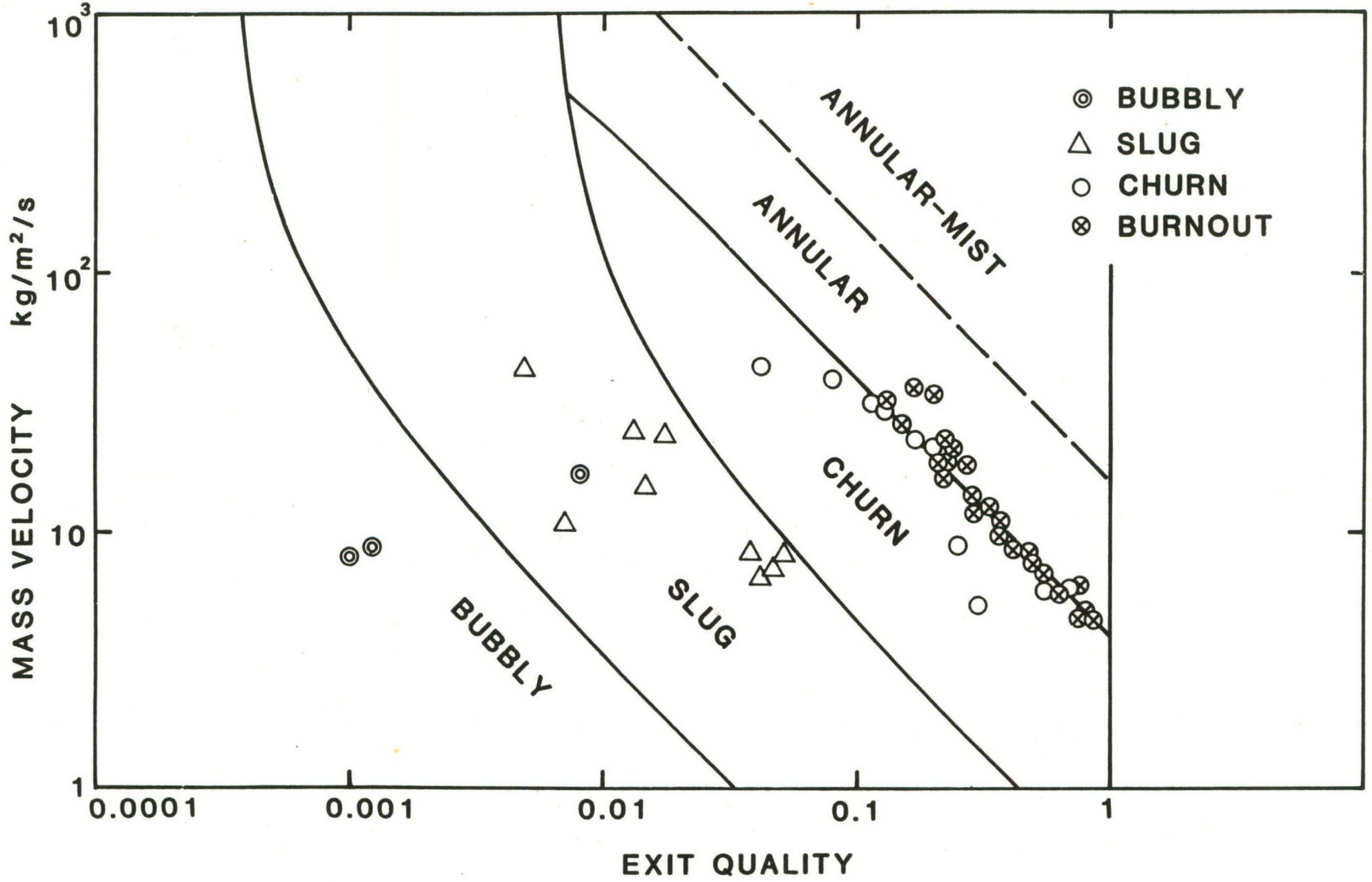

Fig. 4. Test Conditions Plotted in a Flow Regime Map Based on the Criteria of Ishii and Mishima[5]

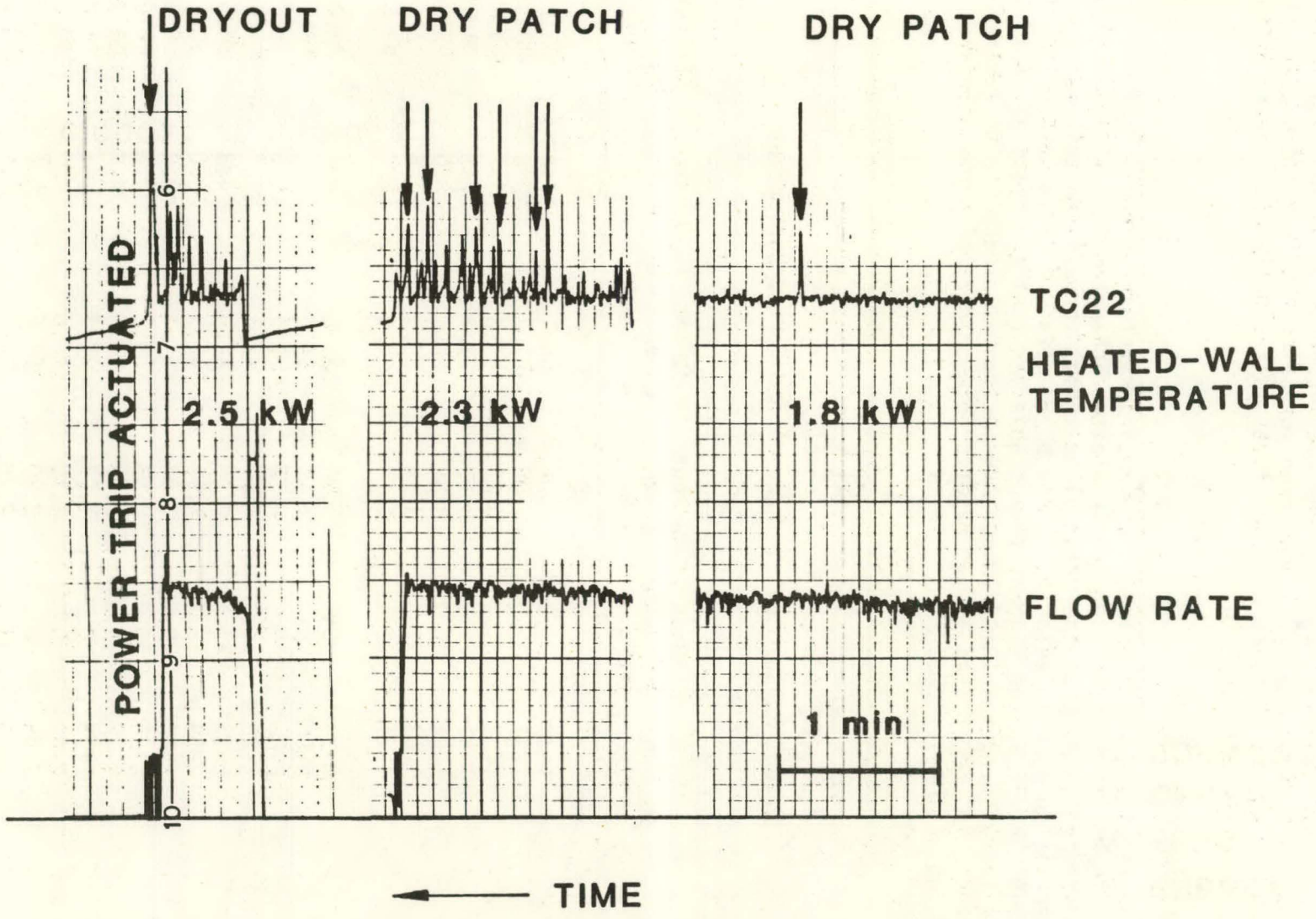

Fig. 5. Typical Heated-wall Temperature and Flow Rate Traces Resulted in a Dryout

of the heated-wall temperature during the dryout is shown in Fig. 5. Some investigators pointed out that the burnout at high steam quality was caused by a film dryout in annular flow.[6-9] The same mechanism of burnout was observed also in this study, however, it occurred just after the transition from churn-turbulent to annular flow at very low inlet mass velocity and low pressure. This is exhibited also in Fig. 4.

B. Critical Heat Flux

The results of critical heat flux measurement are given in Table I. The critical power to the test section is plotted against mass velocity in Fig. 6. The figure indicates that the critical heat flux for a given test section is well correlated by mass velocity. Though the effect of inlet subcooling is not shown clearly in the figure, it was observed that the critical heat flux tend to increase as the inlet subcooling increased. There are no remarkable differences in the critical power results between natural convection and forced convection systems.

Table I.

Dryout Measurements - Natural and Forced Convection

	Run No.	Mass Velocity $kg/m^2/s$	Dryout Power KW	Inlet Temperature °C	Exit Quality %	Dryout Heat Flux KW/m^2
Natural Convection	1-36	23.0	3.08	56.1	21.4	80.3
	1-37	23.0	3.08	62.2	22.6	80.3
	1-39	21.2	3.08	55.6	23.8	80.3
	1-41	29.2	3.62	21.7	12.8	94.4
	1-42	29.7	3.59	26.1	13.0	93.6
	1-43	31.2	3.58	26.1	11.6	93.4
	1-44	32.1	3.59	35.6	12.7	93.6
	2-3	0	1.84	21.5	-	48.0
	2-6	0	1.69	24.5	-	44.1
	2-8	10.1	2.52	26.3	41.5	65.7
	2-10	6.3	1.97	49.1	59.7	51.4
	2-13	11.3	2.28	47.4	34.8	59.5
	2-15	6.1	1.92	48.5	60.0	50.1
	2-24	5.99	1.87	51.7	60.0	48.8
	2-28	10.0	2.53	29.2	42.8	66.0
	2-32	6.3	2.48	29.5	73.9	64.7
	2-38	0	1.77	30.3	-	46.2
	2-41	0	1.70	47.6	-	44.3
	2-45	6.1	2.20	51.2	70.6	57.9
	2-49	11.1	2.26	53.8	36.4	58.9
	2-50	10.9	2.23	34.0	33.0	58.2
	2-51	10.4	2.22	37.6	35.6	57.9
	2-52	9.2	2.07	45.2	29.6	54.0

Table I. (Cont'd)

Dryout Measurements - Natural and Forced Convection

	Run No.	Mass Velocity $kg/m^2/s$	Dryout Power KW	Inlet Temperature °C	Exit Quality %	Dryout Heat Flux KW/m^2
	2-53	7.8	1.91	47.5	44.4	49.8
	2-54	5.7	1.85	48.6	62.2	48.2
Forced Convection	3-1	18.5	3.41	25.2	27.0	88.9
	3-2	30.6	3.64	30.4	13.3	94.9
	3-4	33.6	4.64	47.4	20.7	121.0
	3-5	5.0	1.94	23.1	72.0	50.6
	3-6	7.5	2.23	26.0	51.5	58.2
	3-7	16.2	2.57	29.6	22.0	67.0
	3-8	11.9	2.24	29.7	28.7	58.4
	3-9	18.1	2.80	30.3	21.2	73.0
	3-10	26.2	3.22	34.1	15.0	84.0
	3-11	35.7	4.05	57.1	17.1	105.6
	3-12	4.6	1.96	60.5	85.9	51.1
	3-13	10.4	2.20	-	-	57.4
	3-14	7.2	2.08	52.6	54.9	54.2
	3-15	14.0	2.36	51.6	28.3	61.6
	3-16	22.2	2.56	51.7	16.5	66.8
	3-17	20.1	2.57	53.8	19.7	67.0
	3-18	35.3	4.51	59.3	20.6	117.6
	3-19	0	1.77	52.9	-	46.2
	3-20	5.0	1.89	56.4	75.9	49.3
	3-21	8.3	2.07	55.2	46.9	54.0
	3-22	12.5	2.36	54.4	33.1	61.6
	3-23	18.7	2.65	53.8	22.7	69.1
	3-24	35.8	3.95	58.2	16.6	103.0
	3-25	9.8	2.22	24.1	36.2	57.9
	3-26	8.6	2.20	24.6	42.4	57.4
	3-27	7.7	2.14	26.1	47.9	55.8
	3-28	6.7	2.08	26.3	54.6	54.2
	3-29	5.9	1.98	27.1	61.1	51.6
	3-30	4.6	1.87	27.1	75.6	48.8
	3-31	0	1.74	27.4	-	45.4
	3-32	0	1.73	26.8	-	45.1
	3-33	5.6	1.98	27.2	64.8	51.6
	3-34	6.9	2.03	29.2	52.2	52.9
	3-35	8.6	2.03	33.7	40.1	52.9

It is also suggested that there is a threshold heat flux for burnout to occur. The visual observation in this study confirmed that the occurrence of burnout at zero net flow is closely related to the flooding phenomenon at the

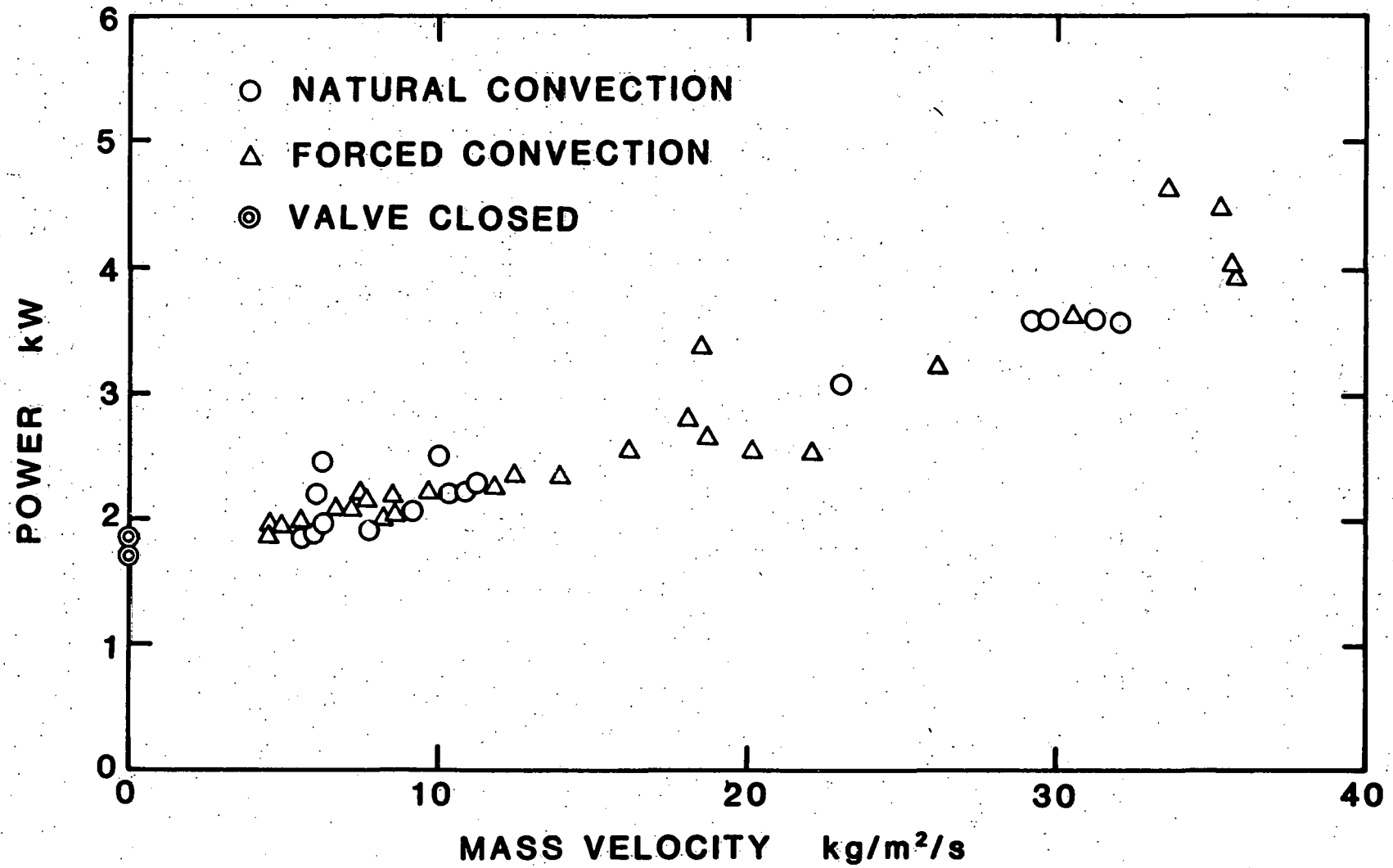

Fig. 6. Critical Power to the Test Section as a Function of Mass Velocity

upper end of the test section.[3, 10-15] The critical power to the test section can be estimated using the Wallis correlation for flooding as follows,[13, 16]

$$j_g^{*1/2} + j_f^{*1/2} = C \tag{1}$$

where

$$j_g^* = j_g \sqrt{\frac{\rho_g}{g\Delta\rho D}} \tag{2}$$

$$j_f^* = j_f \sqrt{\frac{\rho_f}{g\Delta\rho D}} \ . \tag{3}$$

The numerical value of C is 0.725 for sharp edged entrances and 0.88 to 1.0 for rounded entrances respectively. Assuming that the incoming liquid is saturated, we obtain,

$$Q = A\, h_{fg}\, \rho_g\, j_g \ . \tag{4}$$

Equations (1) through (4) yield the following result for the flooding limited power to the test section.

$$Q = \frac{C^2\, h_{fg}\, A\sqrt{\rho_g g\Delta\rho D}}{\left[1 + (\rho_g/\rho_f)^{1/4}\right]^2} \ . \tag{5}$$

From Eq. (5) the critical power to the test section is estimated to be 1.0 to 1.9 KW which agrees well with the results shown in Fig. 6.

As was mentioned in the previous section, the burnout at low mass velocities occurred due to churn-to-annular transition. The criterion for the transition has been developed previously[5, 17] based on the flow reversal within the liquid film at the churn flow bubble section. Therefore,

$$j_g \sqrt{\frac{\rho_g}{g\Delta\rho D}} = \alpha - 0.11 \qquad (\alpha \geq \alpha_m) \tag{6}$$

where

$$\alpha_m = 1 - 0.813 \left[\frac{(C_o - 1)j + 0.35\sqrt{g\Delta\rho D/\rho_f}}{j + 0.75\sqrt{g\Delta\rho D/\rho_f}\left(\frac{g\Delta\rho D^3}{\rho_f \nu_f^2}\right)^{1/18}} \right]^{0.75} \ . \tag{7}$$

Here void fraction α is given based on the drift velocity for churn-turbulent flow as

$$\alpha = \frac{j_g}{C_o\, j + \sqrt{2}\left(\frac{\sigma g \Delta\rho}{\rho_f^2}\right)^{1/4}} \quad . \tag{8}$$

C_o is the distribution parameter[17] and can be given by

$$C_o = 1.2 - 0.2\sqrt{\rho_g/\rho_f} \text{ for a pipe.} \tag{9}$$

The energy balance in the test section is expressed by

$$Q = (h_{fg}\, \rho_g\, j_g + \Delta h_i\, G)A \quad . \tag{10}$$

Using the relationship for j_g, j_f and j, and from Eq. (10), the following equations can be derived,

$$j_g = \frac{Q}{Ah_{fg}\rho_g} - \frac{\Delta h_i}{h_{fg}}\frac{G}{\rho_g} \tag{11}$$

$$j = \frac{Q\Delta\rho}{Ah_{fg}\rho_g\rho_f} + \left(1 - \frac{\Delta h_i}{h_{fg}}\frac{\Delta\rho}{\rho_g}\right)\frac{G}{\rho_f} \quad . \tag{12}$$

Now we use the following non-dimensional groups,

$$q^* \equiv \frac{Q}{h_{fg}\, A_h \sqrt{\lambda\rho_g g\Delta\rho}} \tag{13}$$

$$G^* \equiv \frac{G}{\sqrt{\lambda\rho_g g\Delta\rho}} \tag{14}$$

$$D^* = \frac{D}{\lambda} \tag{15}$$

where λ is the Taylor wave length scale given by

$$\lambda = \sqrt{\frac{\sigma}{g\Delta\rho}} \quad . \tag{16}$$

Here, A_h is the total heat transfer area. The non-dimensional group Eq. (13) is originally derived by Zuber[18] and Kutateladze[19] from the consideration on the hydraulic instability. Using Eqs. (13) through (16), Eqs. (11) and (12) can be rewritten as

$$j_g = J\sqrt{\frac{\lambda g \Delta\rho}{\rho_g}} \tag{17}$$

$$j = \left(J\frac{\Delta\rho}{\rho_f} + \frac{\rho_g}{\rho_f}G^*\right)\sqrt{\frac{\lambda g\Delta\rho}{\rho_g}} \tag{18}$$

where

$$J \equiv q^*\frac{A_h}{A} - \frac{\Delta h_i}{h_{fg}}G^* \quad . \tag{19}$$

In this study, $\Delta h_i/h_{fg}$ was large enough compared to $\rho_g/\Delta\rho$, then the second term on the right hand side of Eq. (18) can be neglected.

$$j \simeq J\sqrt{\frac{\lambda g\Delta\rho}{\rho_g}}\frac{\Delta\rho}{\rho_f} \quad . \tag{20}$$

Finally, from Eqs. (6) and (8) we obtain,

$$J \equiv \sqrt{D^*}\left(\frac{J}{C_o J\frac{\Delta\rho}{\rho_f} + \sqrt{\frac{2\rho_g}{\rho_f}}} - 0.11\right) \quad . \tag{21}$$

Equation (21) can be solved with the condition $\alpha > \alpha_m$ to give

$$J = \frac{1}{2}\left(\frac{\rho_f\sqrt{D^*}}{C_o\Delta\rho} - \frac{\sqrt{2\rho_f\rho_g}}{C_o\Delta\rho} - 0.11\sqrt{D^*}\right)$$

$$+ \frac{1}{2}\left[\left(\frac{\rho_f\sqrt{D^*}}{C_o\Delta\rho} - \frac{\sqrt{2\rho_f\rho_g}}{C_o\Delta\rho} - 0.11\sqrt{D^*}\right)^2 - 0.4\frac{\sqrt{2D^*\rho_f\rho_g}}{C_o\Delta\rho}\right]^{1/2} \quad . \tag{22}$$

For low pressure steam-water flow, ρ_g/ρ_f can be neglected in Eq. (22) and $\Delta\rho \simeq \rho_f$, then

$$J \simeq \frac{1}{C_o} - 0.11 \sqrt{D^*} \tag{23}$$

or more explicitly,

$$q^* = \frac{A}{A_h}\left[\frac{\Delta h_i}{h_{fg}} G^* + \left(\frac{1}{C_o} - 0.11\right)\sqrt{D^*}\right] . \tag{24}$$

In terms of the critical heat flux it becomes

$$q''_c = \frac{A}{A_h}\left[\Delta h_i\, G + \left(\frac{1}{C_o} - 0.11\right) h_{fg}\sqrt{\rho_g \Delta\rho g D}\right] . \tag{25}$$

Comparison of q^* predicted by Eq. (24) with the experimental data can be found in Fig. 7 which shows a reasonable agreement between them.

IV. DISCUSSION AND GENERALIZED CORRELATION

A. Burnout Mechanism

Barnard et al.[20] investigated dryout at low flow rate for an upward flow of Freon-113 in a vertical tube. They classified the burnout mechanisms into five types. When the flow passages are substantially filled with liquid, the burnout will occur due to the vapor production by boiling which prevents liquid from reaching the heated surface. This is the well-known pool boiling burnout. Flooding limited burnout occurs at zero net flow through the flow passage when the vapor flow prevents a sufficient downward flow of liquid. When the flow rate through the flow passage is not zero but very low, all the liquid entering into the passage from the bottom will be evaporated and the vapor flow will prevent liquid flowing down from the top. This type of burnout is called a circulation and flooding limited burnout. As the flow rate from the bottom increases, the vapor flow becomes sufficiently high to prevent any liquid flowing down the flow passage from the top. In this case, the dryout occurs when the vapor quality approaches 100%. This is called a circulation limited burnout. For higher flow rates, a substantial amount of the liquid will be entrained by the vapor flow, which causes dryout at vapor qualities less than 100%. This is so called entrainment limited burnout. The last two types have often been referred to as a basic mechanism of burnout in annular two-phase flow.[6-9]

However, the observation in this study indicated the possibility of burnout caused by the flow regime transition from churn-turbulent to annular flow as was discussed in the previous section. This type of burnout occurred over the same range of mass velocity as circulation limited burnout. At present boundary between these different types of burnout cannot be predicted with high certainty. It will be interesting to note that film dryout on the heated wall did cause the burnout but liquid film still remained on the unheated wall in case of the annulus test section during this type of burnout.

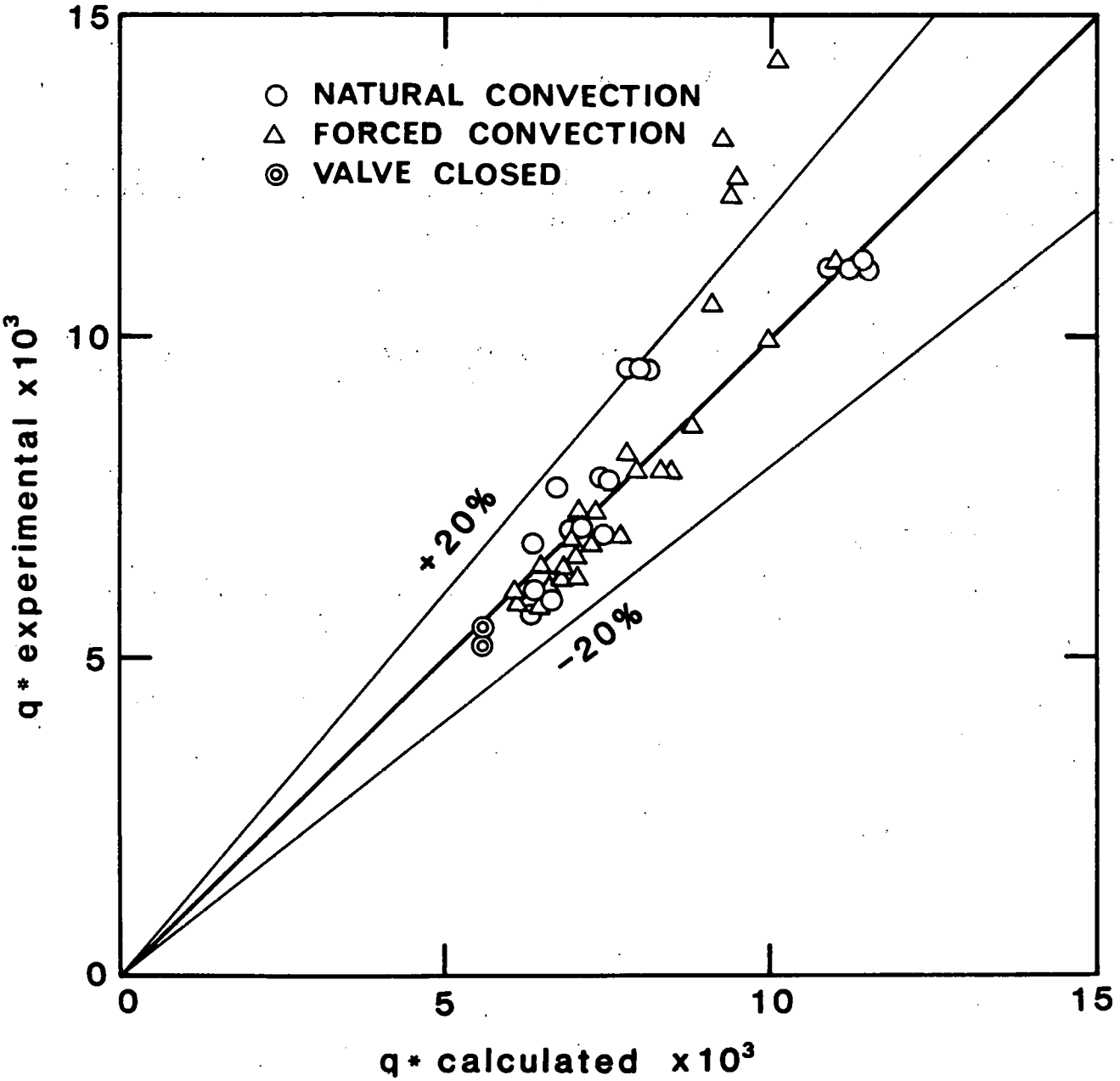

Fig. 7. Comparison of Predicted Non-dimensional Flux q^* with the Experimental Data

B. Generalized Correlation for CHF

1. Pool Boiling Burnout

Zuber[18] and Kutateladze[19] proposed essentially the same correlation for pool boiling burnout as follows:

$$q = K\, h_{fg}\, \rho_g \left(\frac{\sigma g^2 \Delta\rho}{\rho_g^2}\right)^{1/4} \left(\frac{\rho_f}{\rho_f + \rho_g}\right)^n \quad . \tag{26}$$

Zuber derived this equation from the consideration on the stability of vapor-liquid interface.[18] On the other hand, Kutateladze obtained it by correlating data using non-dimensional parameters. Thus he found that

$$K = 0.14 \text{ and } n = 0 \quad .$$

Then, Eq. (26) can be rewritten by using the non-dimensional groups defined by Eqs. (13)-(16) as

$$q^* = 0.14 \quad . \tag{27}$$

2. Flooding Limited Burnout

The heat flux at burnout caused by flooding can be calculated by Eq. (5), which is expressed in a non-dimensional form as follows,

$$q^* = C^2 \zeta \tag{28}$$

where

$$\zeta \equiv \frac{A\sqrt{D^*}}{A_h\left(1 + \sqrt[4]{\rho_g/\rho_f}\right)^2} \quad . \tag{29}$$

In terms of the critical heat flux, this criterion becomes

$$q_c = \frac{A}{A_h} \frac{C^2\, h_{fg} \sqrt{\rho_g \Delta\rho g D}}{\left(1 + \sqrt[4]{\rho_g/\rho_f}\right)^2} \quad . \tag{30}$$

A reasonable agreement between Eq. (28) and the experimental data under various conditions[3, 10, 11, 20] is shown in Fig. 8. As Block and Wallis[13] pointed out, the burnout heat flux tends to be constant for small L/D which means that the burnout is limited by wall heat flux. Then it may be deduced that pool

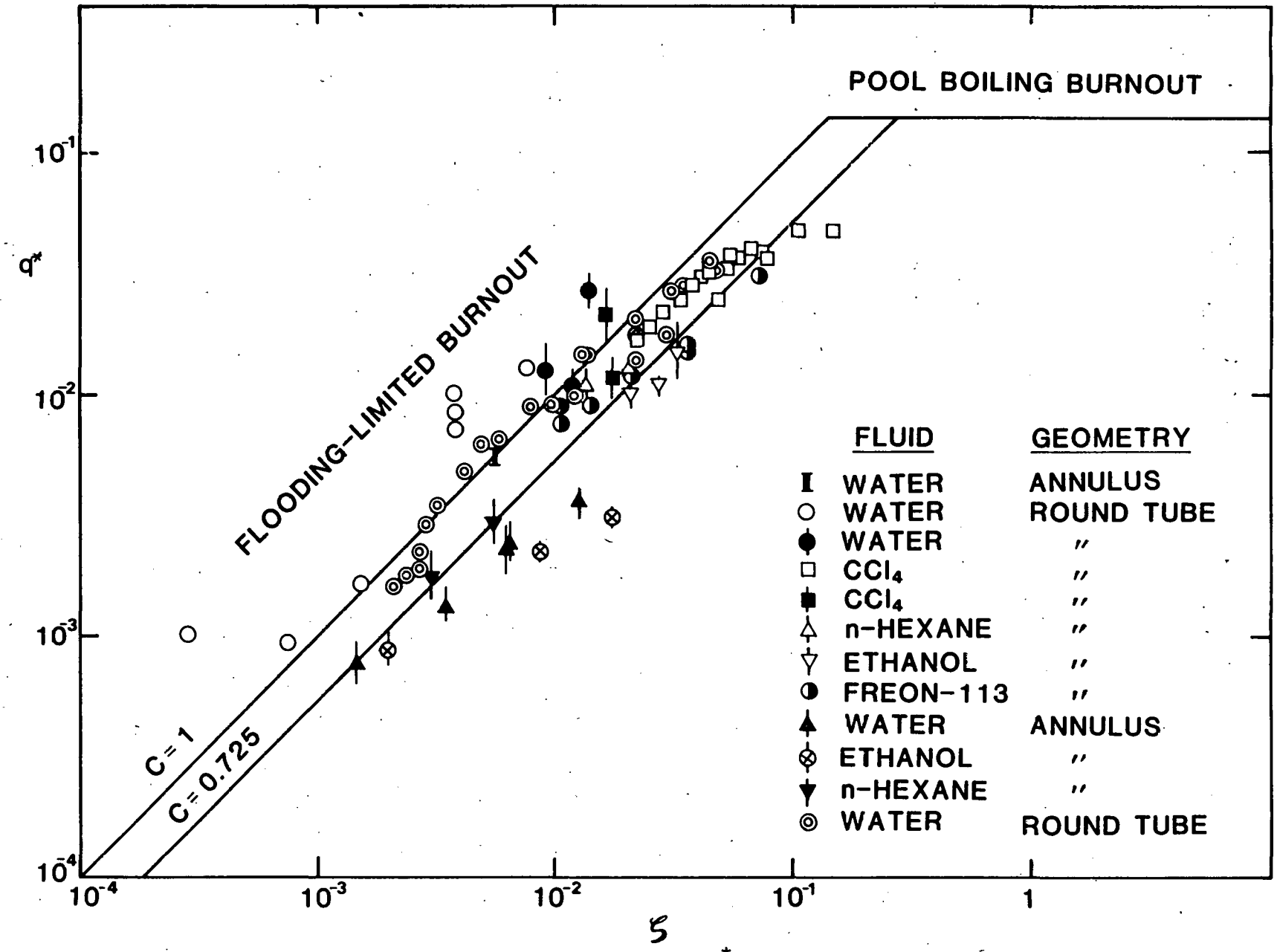

Fig. 8. Non-dimensional Burnout Heat Flux q^* versus ζ for Flooding Limited Burnout

boiling type burnout will occur in very short tubes. The transition from pool boiling type to flooding limited burnout can be calculated from Eqs. (27) and (28) as

$$C^2\zeta = 0.14 \quad . \tag{31}$$

Thus the non-dimensional burnout heat flux q^* for these two regimes can be given as a function of ζ as illustrated in Fig. 8.

In the previous section, Eq. (24) was derived as a burnout heat flux caused by churn-to-annular flow transition. The criterion for the transition is based on the assumption that liquid film flow changes the direction from downward to upward at transition. Then, when $G^* = 0$ in Eq. (24), it should give the flooding condition. Actually, when $G^* = 0$, Eq. (24) becomes

$$q^* = \frac{A}{A_h}\left(\frac{1}{C_o} - 0.11\right)\sqrt{D^*} \quad . \tag{32}$$

Comparing Eqs. (28), (29) and (32), we obtain

$$C^2 = \left(\frac{1}{C_o} - 0.11\right)\left(1 + \sqrt[4]{\rho_g/\rho_f}\right)^2 \quad . \tag{33}$$

For water under atmospheric pressure, the numerical value of the right hand side in Eq. (33) is 0.97 which agrees well with that of C^2 given by Wallis.

Furthermore, in a very rapid transient it can be considered that the flow may not develop to the flooding condition. In such a case, the pool boiling type CHF criterion may still be used for a short time period.

3. Circulation and Flooding Limited Burnout

The physical model for this regime is illustrated in Fig. 9. Now we postulate that all the liquid entering into the flow passage from the bottom is evaporated and the liquid from the top is limited by flooding due to high steam flow, resulting in a dryout on the heated surface. The heat balance can be expressed as,

$$Q = A(h_{fg}\,\rho_g\,j_g + \Delta h_i\,G) \tag{34}$$

and

$$\rho_g j_g = \rho_g\,j_{gc} + \rho_f j_f \quad . \tag{35}$$

Here $\rho_f j_f$ is the liquid flux from the top and $\rho_g j_{gc}$ is the total evaporated mass flux from the bottom. From the assumption that all the liquid entering from the bottom is evaporated, we obtain

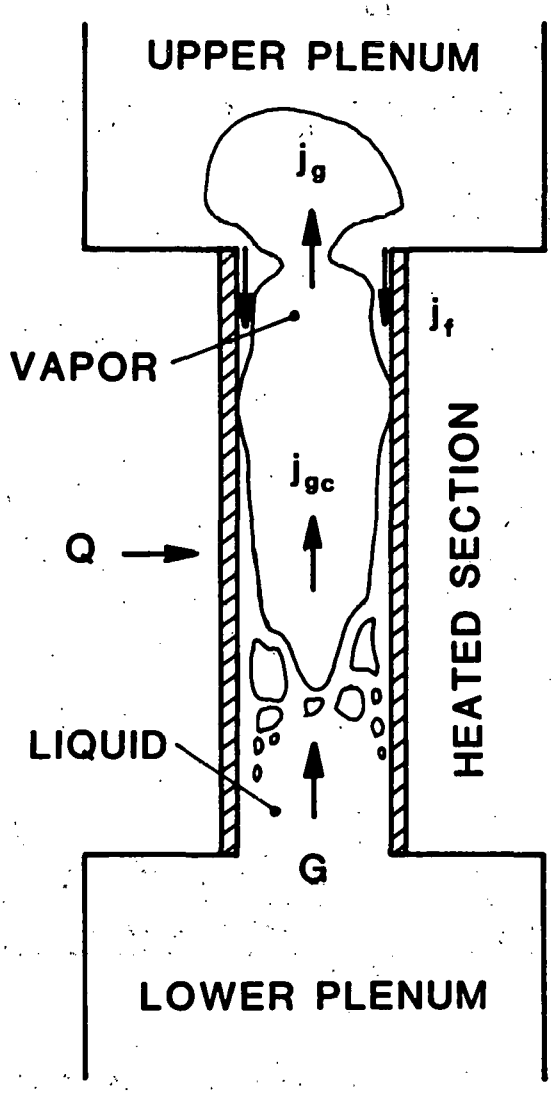

Fig. 9. Model for Circulation and Flooding Limited Burnout

$$G = \rho_g j_{gc} \quad . \tag{36}$$

Using non-dimensional groups defined previously, Eqs. (1), (35) and (36) yield,

$$(1 - \sqrt{\rho_g/\rho_f})\, j_g^* - 2C j_g^{*1/2} + \frac{G^*}{\sqrt{D^*}} \sqrt{\frac{\rho_g}{\rho_f}} + C^2 = 0 \quad . \tag{37}$$

Equation (37) is a quadratic form of $j_g^{*1/2}$ and has real solutions if

$$C^2 \geq (1 - \sqrt{\rho_g/\rho_f})\, G^* \sqrt{D^*} \quad . \tag{38}$$

Inequality (36) is met when

$$j_f^* = \left(j_g^* - \frac{G^*}{\sqrt{D^*}} \right) \sqrt{\rho_g/\rho_f} \geq 0 \quad . \tag{39}$$

Equations (1)-(3) require that

$$j_g^{*1/2} = \frac{C}{1 + \sqrt[4]{\rho_g/\rho_f}} \tag{40}$$

when G^* approaches to zero. Therefore, we arrive at the solution

$$j_g^{*1/2} = \frac{C - \sqrt{C^2 \sqrt{\rho_g/\rho_f} - (1 - \sqrt{\rho_g/\rho_f})\, G^* \sqrt{\rho_g/(\rho_f D^*)}}}{1 - \sqrt{\rho_g/\rho_f}} \quad . \tag{41}$$

Finally, non-dimensional heat flux is derived by using Eq. (34), (41) and the definition of non-dimensional groups.

$$q^* = \frac{A\sqrt{D^*}}{A_h} \left[\left(\frac{C}{1 + \sqrt[4]{\rho_g/\rho_f}} \right)^2 \left(\frac{1 - \sqrt[4]{\rho_g/\rho_f} \sqrt{1 - (\sqrt{\rho_f/\rho_g} - 1)\, G^* \sqrt{\rho_g/(\rho_f D^*)}/C^2}}{1 - \sqrt[4]{\rho_g/\rho_f}} \right)^2 + \frac{\Delta h_i}{h_{fg}} \frac{G^*}{\sqrt{D^*}} \right] . \tag{42}$$

4. Circulation Limited Burnout

This type of burnout is characterized by 100% evaporation of the liquid entering from the bottom and no liquid flow from the top. Therefore, letting

$$j_f^* = \left(j_g^* - \frac{G^*}{\sqrt{D^*}}\right)\sqrt{\rho_g/\rho_f} = 0 \tag{43}$$

and

$$j_g^* = C^2 \tag{44}$$

in Eq. (39), we obtain for the burnout heat flux,

$$q^* = \frac{A}{A_h} G^* \left(1 + \frac{\Delta h_i}{h_{fg}}\right) . \tag{45}$$

5. Entrainment Limited Burnout

There have been some attempts to calculate the burnout heat flux in this regime using annular flow model.[7-9] Whalley et al.[21] obtained an encouraging result from their analysis. However, no generalized correlation has been presented in a closed form. An example of entrainment limited burnout was given by Barnard et al. for Freon-113.[20] They explained their experimental results successfully using annular flow model of Whalley et al.[21] with a simple empirical equation for entrainment fraction. Their data on mass velocity versus vapor quality at burnout are plotted in Fig. 10, compared with the flow regime map predicted by the authors.[5] The figure shows that the most of the burnouts occurred in annular-mist flow which is consistent with the observation in Reference 20. The relationship between burnout heat flux and mass velocity for Freon-113 is shown in non-dimensional form in Fig. 11. Some non-dimensional correlations also appear in the figure.

The Katto correlation was developed from a wide variety of experimental data for forced convection burnout in round tubes using dimensional analysis.[22] The L-regime correlation is given by

$$\frac{q}{h_{fg}G} = C_l \left(\frac{\sigma\rho_f}{G^2 L}\right)^{0.043} \frac{D}{L}\left(1 + 1.16\,\frac{\Delta h_i}{h_{fg}}\right) \tag{46}$$

where $C_l = 0.25$ or $C_l = 0.34$ for Freon, or in a non-dimensional form used in this study,

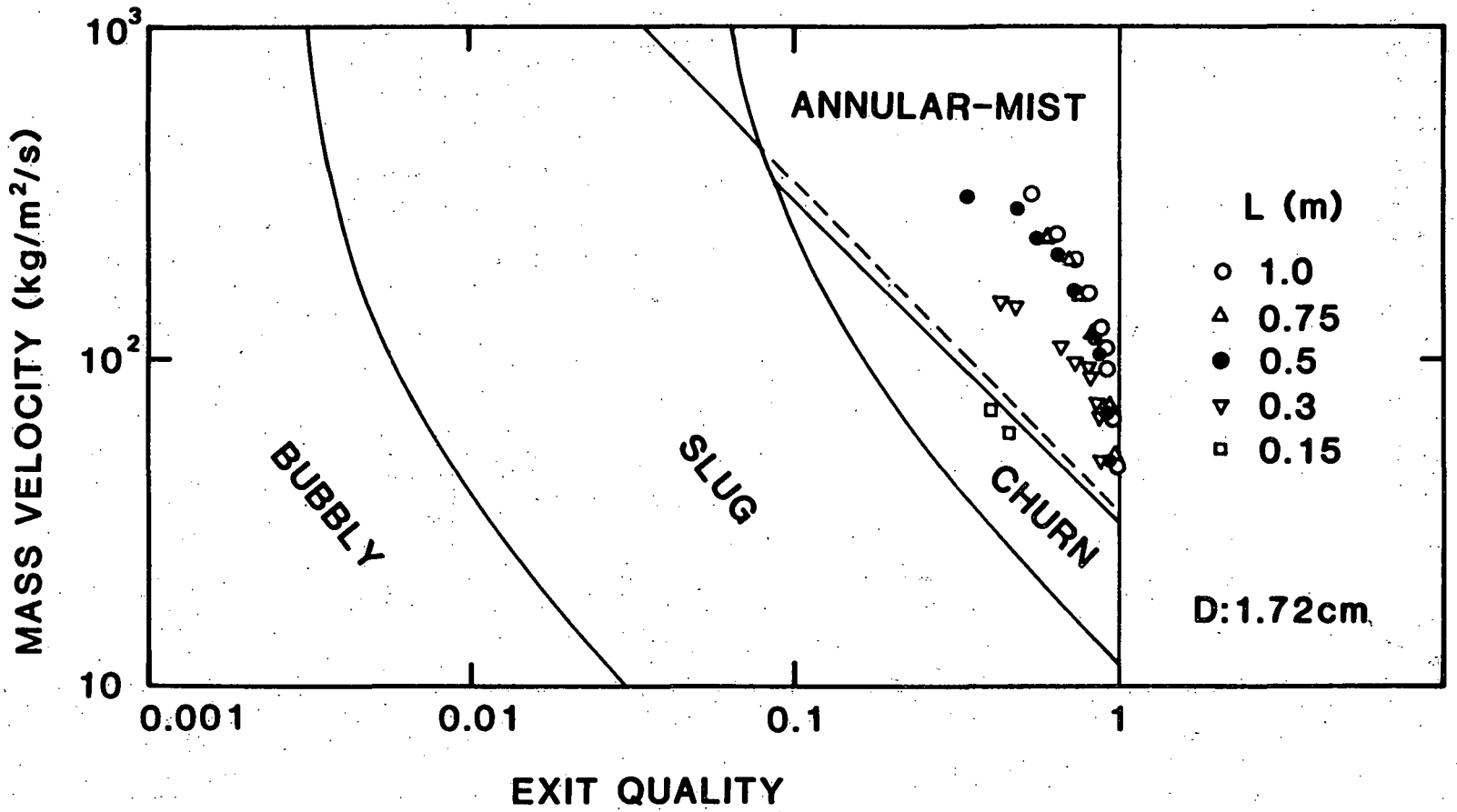

Fig. 10. Burnout Data of Barnard et al.[20] Plotted in the Flow Regime Map Based on the Criteria of Ishii and Mishima[5]

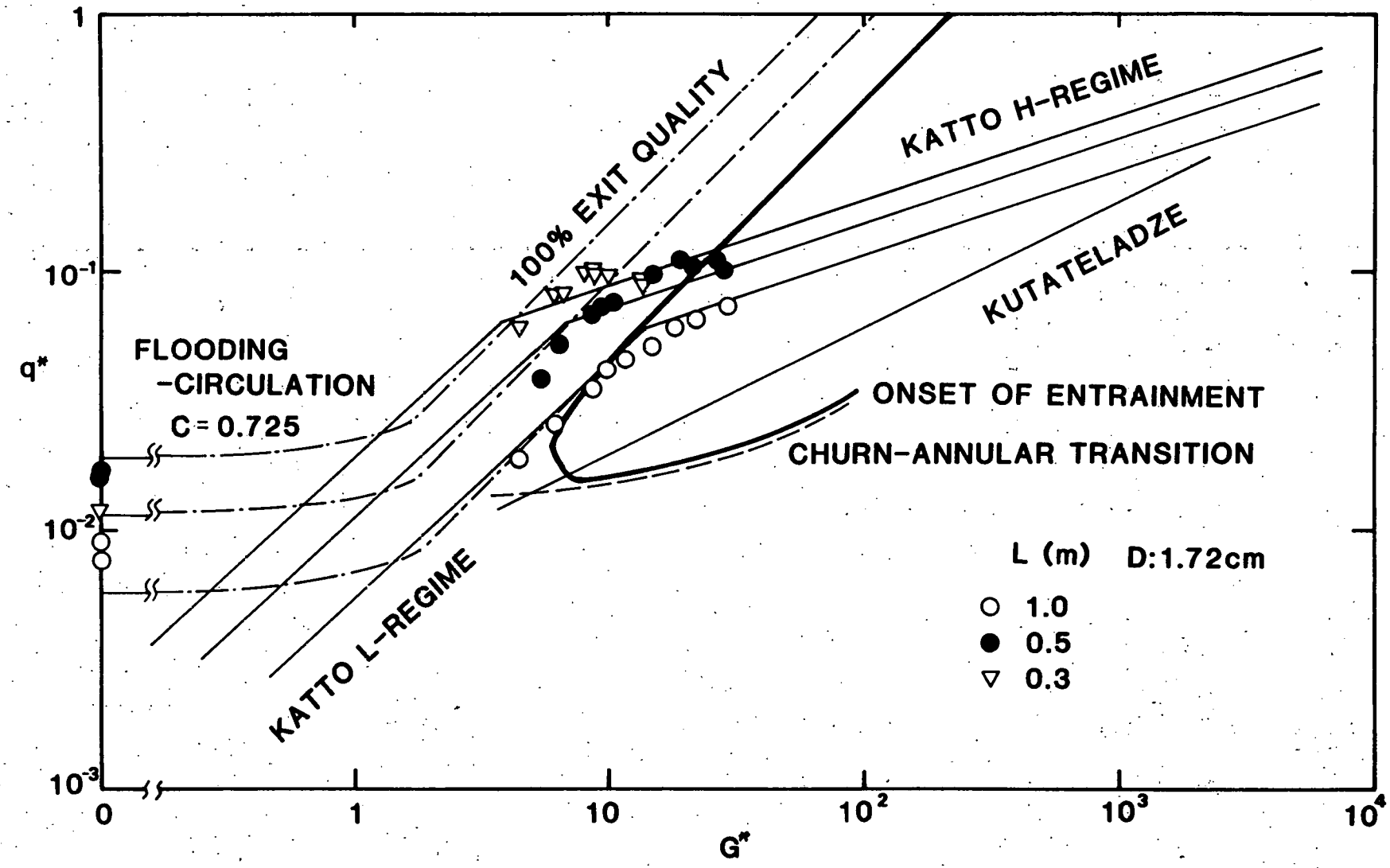

Fig. 11. Freon-113 Burnout Heat Flux Data Compared with Several Correlations

$$q^* = C_1 \frac{D}{L}\left(\frac{\rho_f \lambda}{\rho_g L}\right)^{0.043} G^{*0.914}\left(1 + 1.16\,\frac{\Delta h_i}{h_{fg}}\right) . \qquad (47)$$

Equation (47) is similar to Eq. (45) as the term $(\rho_f\lambda/\rho_g/L)^{0.043}$ is close to unity over the experimental range. This agrees with Katto's description that the burnout in L-regime is caused mainly by the dryout of an annular liquid film on the heated surface when the fraction of liquid entrained in the gas core is small. Another Katto correlation is, for H-regime,

$$\frac{q}{h_{fg}G} = 0.1\left(\frac{\rho_g}{\rho_f}\right)^{0.133}\left(\frac{\sigma\rho_f}{G^2 L}\right)^{1/3}\frac{1 + K_H\,\Delta h_i/h_{fg}}{1 + 0.0031\,L/D} \qquad (48)$$

where

$$K_H = 1.8\left(\frac{L/D}{130}\right)^{-5}\rho_g/\rho_f$$

for $\sigma\rho_f/G^2L < 3 \times 10^{-6}$, and

$$K_H = 0.075\left(\frac{L/D}{130}\right)^{-5}\rho_g/\rho_f\left(\frac{\sigma\rho_f}{G^2 L}\right)^{-1/4} \qquad (49)$$

for $\sigma\rho_f/G^2L > 3 \times 10^{-6}$.

Equation (48) is expressed in an analogous form to Eq. (47) as

$$q^* = 0.1\,G^{*1/3}\left(\frac{\lambda}{L}\right)^{1/3}\left(\frac{\rho_f}{\rho_g}\right)^{0.2}\frac{1 + K_H\,\Delta h_i/h_{fg}}{1 + 0.0031\,L/D} . \qquad (50)$$

Katto explained that the burnout in H-regime is affected by hydrodynamic instability. However, it can be seen from the figure that the entrainment-limited burnout data of Barnard et al.[20] are well reproduced by these correlations. The Kutateladze correlation for low pressure,[23]

$$q^* = 0.023\sqrt[4]{\frac{\rho_g\Delta\rho}{\rho_f^2}}\sqrt{G^*}\left[1 + 0.4505\left(\frac{\rho_f}{\rho_g}\right)^{0.85}\frac{\Delta h_{BO}}{h_{fg}}\right] \qquad (51)$$

is also compared with the experimental data in Fig. 11, which shows that Eq. (51) predicts lower burnout heat fluxes over the experimental range for Freon-113. Here Δh_{BO} is the enthalpy subcooling at burnout location.

The broken lines in Fig. 11 exhibit the churn-to-annular flow transition boundaries predicted by Eq. (24). The equation was derived assuming that $\Delta h_i/h_{fg}$ is large enough compared to $\rho_g/\Delta\rho$. The test condition of Barnard et al.[20] satisfies this condition so that Eq. (24) may be used as a first approximation. However, the figure shows that the measured burnout heat fluxes are far above the churn-to-annular transition boundary. The bold line in Fig. 11 corresponds to the onset of entrainment based on the criterion developed by Ishii et al.[24] According to the criterion, liquid entrainment will occur when the following inequalities are met,

$$\frac{\mu_f j_g}{\sigma}\sqrt{\frac{\rho_g}{\rho_f}} > 11.78\, N_\mu^{0.8}\, Re_f^{-1/3} \tag{52}$$

for $Re_f < 1635$, and

$$\frac{\mu_f j_g}{\sigma}\sqrt{\frac{\rho_g}{\rho_f}} > N_\mu^{0.8} \tag{53}$$

for $Re_f > 1635$ where N_μ is a viscosity number defined by

$$N_\mu = \frac{\mu_f}{\sqrt{\rho_f \sigma \lambda}} \tag{54}$$

and

$$Re_f = \frac{\rho_f j_f D}{\mu_f} \quad . \tag{55}$$

Inequalities (52) and (53) can be rewritten by using the definition of non-dimensional groups Eqs. (13)-(16) and Eq. (10) as,

$$J(G^* - J)^{1/3} > 11.78\, N_\mu^{2/15}\, D^{*-1/3} \left(\frac{\rho_f}{\rho_g}\right)^{1/6} \tag{56}$$

for $Re_f < 1635$, and

$$J > N_\mu^{-0.2} \tag{57}$$

for $Re_f > 1635$ where J is defined by Eq. (19). Inequality (56) can be solved numerically by an iterative calculation. A rough estimate, however, can be obtained from the following expression, though it gives only a necessary condition for Inequality (56).

$$q^* < \frac{A}{A_h}\left[\left(1 + \frac{\Delta h_i}{h_{fg}}\right) G^* - \frac{1.63 \times 10^3}{G^{*3}} N_\mu^{2/5} D^{*-1} \sqrt{\frac{\rho_f}{\rho_g}}\right] . \qquad (58)$$

Inequality (57) also can be rewritten more explicitly as,

$$q^* > \frac{A}{A_h}\left[\frac{\Delta h_i}{h_{fg}} G^* + N_\mu^{-0.2}\right] . \qquad (59)$$

As shown in Fig. 11, Inequalities (56) and (57) predict an onset of entrainment very close to the churn-to-annular flow transition for this case.

C. Discussion

The experimental data obtained from this study are compared with the generalized correlations described above in Fig. 12. Some other correlations for water also will be found in the figure. Those correlations[25-29] are summarized in Table 2. The Macbeth correlation[25, 26] and the Lowdermilk correlation[27] were originally developed for subcooled upward water flow in a round tube. However, they were applied to a water flow in an annulus replacing hydraulic equivalent diameter by heated equivalent diameter which appears in the equations. Their correlation consists of two equations, one is for low velocity regime and the other is for high velocity regime just as L-regime and H-regime respectively of the Katto correlation for annuli.[29] Barnett[28] correlated experimental data for internally heated annuli assuming a Macbeth type of correlation, however, the applicable range is limited to rather high mass velocities.

From Fig. 12 we can see that the data are well correlated by Eq. (24) which was derived from the criterion for churn-to-annular flow transition. The Kutateladze correlation is also close to the data over the experimental range. On the other hand, those correlations listed in Table 2 predict heat fluxes much larger than experimental data, though the correlations agree well with each other. As pointed out in the previous section, these correlations may be used for entrainment-limited burnout. However, Fig. 12 indicates the existence of different mechanism of dryout. The criterion over which mechanism should take place will be subject to further studies. It is interesting to note at present that no entrainment occurred in this case according to the criterion of Ishii[24] as shown by the bold line in Fig. 12 while the onset of entrainment followed just after the churn-to-annular flow transition in the case shown in Fig. 10. Observations in previous works[6-9] revealed that the entrainment and the deposition of liquid droplets could be a controlling factor for film dryout. In other words, we cannot expect droplet quenching in addition to the liquid film remained on the unheated surface in this case.

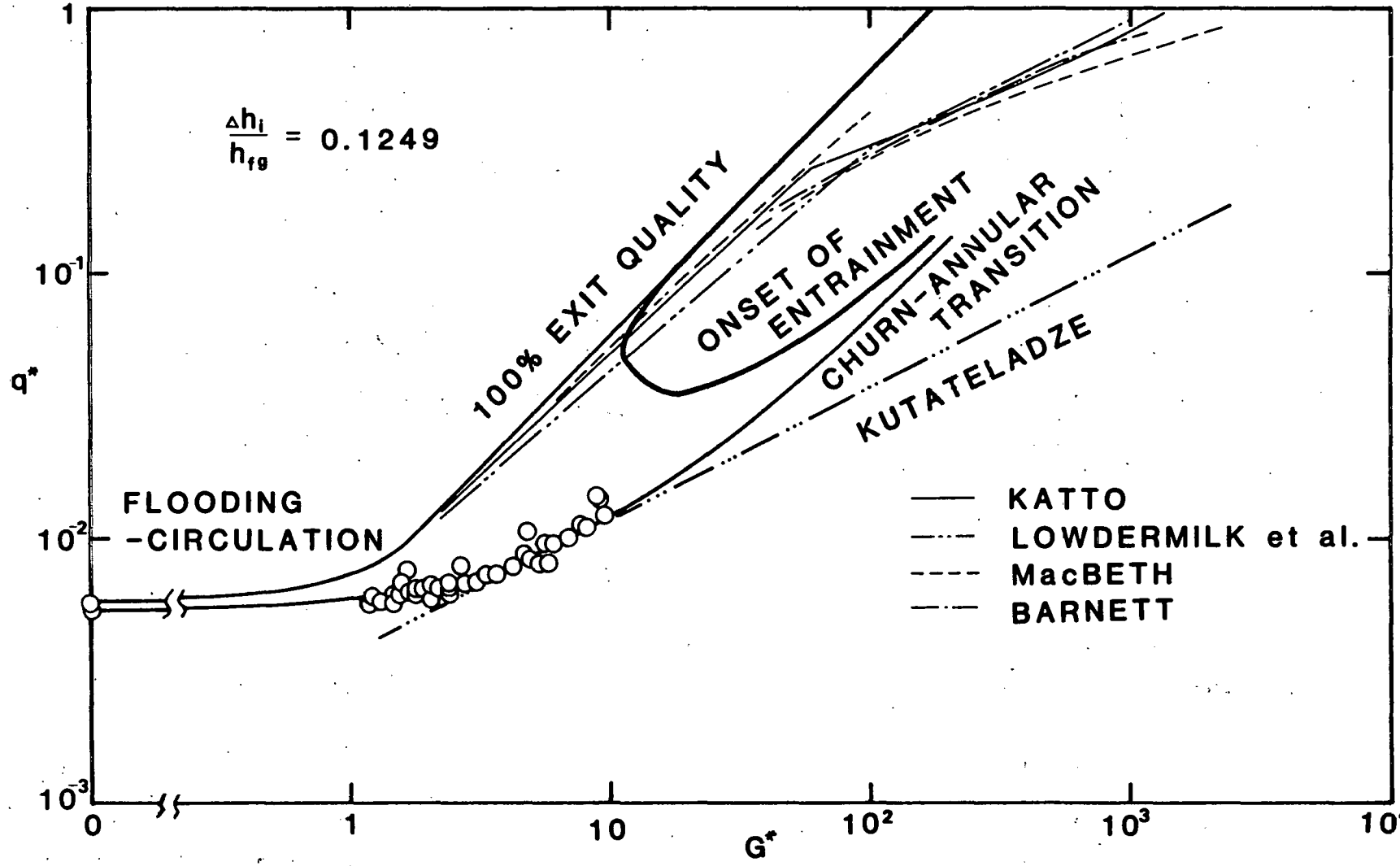

Fig. 12. Comparison of Burnout Correlations at Low Pressure and Low Mass Velocities

Table II

Correlations for Burnout at Low Mass Velocities for Water

Source	Correlations	Applicable Ranges
Macbeth[25, 26]	$q \times 10^{-6} = \frac{A_1 + C_1 D (G \times 10^{-6})\Delta h_i/4}{1 + C_1 L}$	geometry: round tube steam quality: positive
	Low Mass Velocity Region	Low Mass Velocity Region
	$A_1 = 0.00106\ h_{fg}\ D^{-0.63}\ (G \times 10^{-6})^{-0.17}$	D: 0.3 - 1.0 cm L: 0.15 - 3 m G: 14 - 841 $kg/m^2/3$ P: 1 - 138 bar Δh_i: 65 - 1400 kJ/kg
	$C_1 = 0.00344\ D^{-1.73}\ (G \times 10^{-6})^{-1.22}$	
	High Mass Velocity Region	High Mass Velocity Region
	$A_1 = 1.12\ D^{-0.211}\ (G \times 10^{-6})^{0.324}$	D: 0.1 - 2.4 cm L: 0.0254 - 0.86 m L/D: 8.5 - 50 G: 140 - 5750 $kg/m^2/s$ P: ~1 bar
	$C_1 = 0.001\ D^{-1.4}\ (G \times 10^{-6})^{-1.05}$	
	where q: Btu/hft^2, G: lb/hft^2 Δh_i, h_{fg}: Btu/lg L, D: in.	
Lowdermilk, et al.[27]	$G/(L/D)^2 < 150$ $q = 270\ D^{-0.2}\ (L/D)^{-0.85}\ G^{0.85}$ $G/(L/D)^2 > 150$ $q = 1400\ D^{-0.2}\ (L/D)^{-0.15}\ G^{0.50}$ where L, D: ft, the others: same as above	geometry: round tube D: 0.13 - 0.48 cm L/D: 25 - 250 ΔT_{in}: 0 - 80°C P: 1 - 7 bar q: 2.79×10^3 -41.6×10^3 KW/m^3

Table II (Cont'd)

Source	Correlations	Applicable Ranges
Barnett[28]	$q \times 10^{-6} = \frac{A(h_{fg}/649) + B\Delta h_i}{C + L}$ $A = 67.45\, D_h^{0.68}\, (G \times 10^{-6})^{0.192}\, [1 - 0.744\exp(-6.512\, D(G \times 10^{-6}))]$ $B = 0.2587\, D_h^{1.261}\, (G \times 10^{-6})^{0.817}$ $C = 185.0\, D^{1.415}\, (G \times 10^{-6})^{0.212}$ where the units are the same as the Macbeth correlation	geometry: internally heated annulus D_i: 0.95 - 9.65 cm D_o: 1.4 - 10.16 cm L: 0.61 - 2.74 m G: 190 - 8430 kg/m^2/s Δh_i: 0 - 0.958 MJ/Kg P: 41.5 - 96.5 bar
Katto[29]	<u>L-regime</u> $\frac{q}{h_{fg}G} = 0.25 \left(\frac{\sigma\rho_f}{G^2L}\right)^{0.043} \frac{D_h}{L} \left(1 + \frac{\Delta h_i}{h_{fg}}\right)$ <u>H-regime</u> $\frac{q}{h_{fg}G} = 0.12 \left(\frac{\rho_g}{\rho_f}\right)^{0.133} \left(\frac{\sigma\rho_f}{G^2L}\right)^{1/3} \frac{1 + K_H\Delta h_i/h_{fg}}{1 + 0.0081\, L/D_h}$ $K_H = 0.057 \left(\frac{69.2}{L/D_h}\right)^{11.0\rho_g/\rho_f} \left(\frac{\sigma\rho_f}{G^2L}\right)^{-1/3}$	geometry: internally heated annulus <u>L-regime</u> D_o/D_i: 1.04 L: 1.88 m L/D: 24.7 P: 69.0 bar

Another factor that we should consider is the effect of system pressure on the flow regime transition. For example, the Barnett data for water at 69 bars in an annulus with approximately the same hydraulic diameter as the present study can be well reproduced by his correlation,[28] which is very close to the Katto correlation[29] as shown in Fig. 13. It is interesting to note that for this case the occurrence of slug-annular flow transition, instead of churn-annular flow transition, is predicted by the criteria.[5] Therefore, it may be pointed out that such burnout mechanism as was observed in the present study may be a characteristic phenomenon for low pressure system. Furthermore, in relation to the flooding limited burnout, it is expected that a relatively large inlet flow restriction tends to lead to this mode of critical heat flux phenomenon.

V. CONCLUSIONS

An experiment has been performed at low flow rates of steam-water upward flow in an annulus and the data were compared with various correlations. The following conclusions can be derived from the discussions;

a. Burnout heat flux at zero net flow can be predicted by flooding correlation, which gives lower burnout heat fluxes for large L/D than those predicted by pool boiling burnout correlation.

b. Visual observation revealed that the burnout at low mass velocities occurred due to liquid film dryout upon the flow regime transition from churn-turbulent to annular flow.

c. A non-dimensional correlation for the burnout heat flux due to the flow regime transition has been derived from the criterion of Ishii.[17]

d. On the other hand, the conventional correlations for low mass velocities well reproduce the data on circulation and entrainment limited burnout.

e. Further studies are needed to establish the criterion over which regime of burnout should occur at given conditions of low mass velocities.

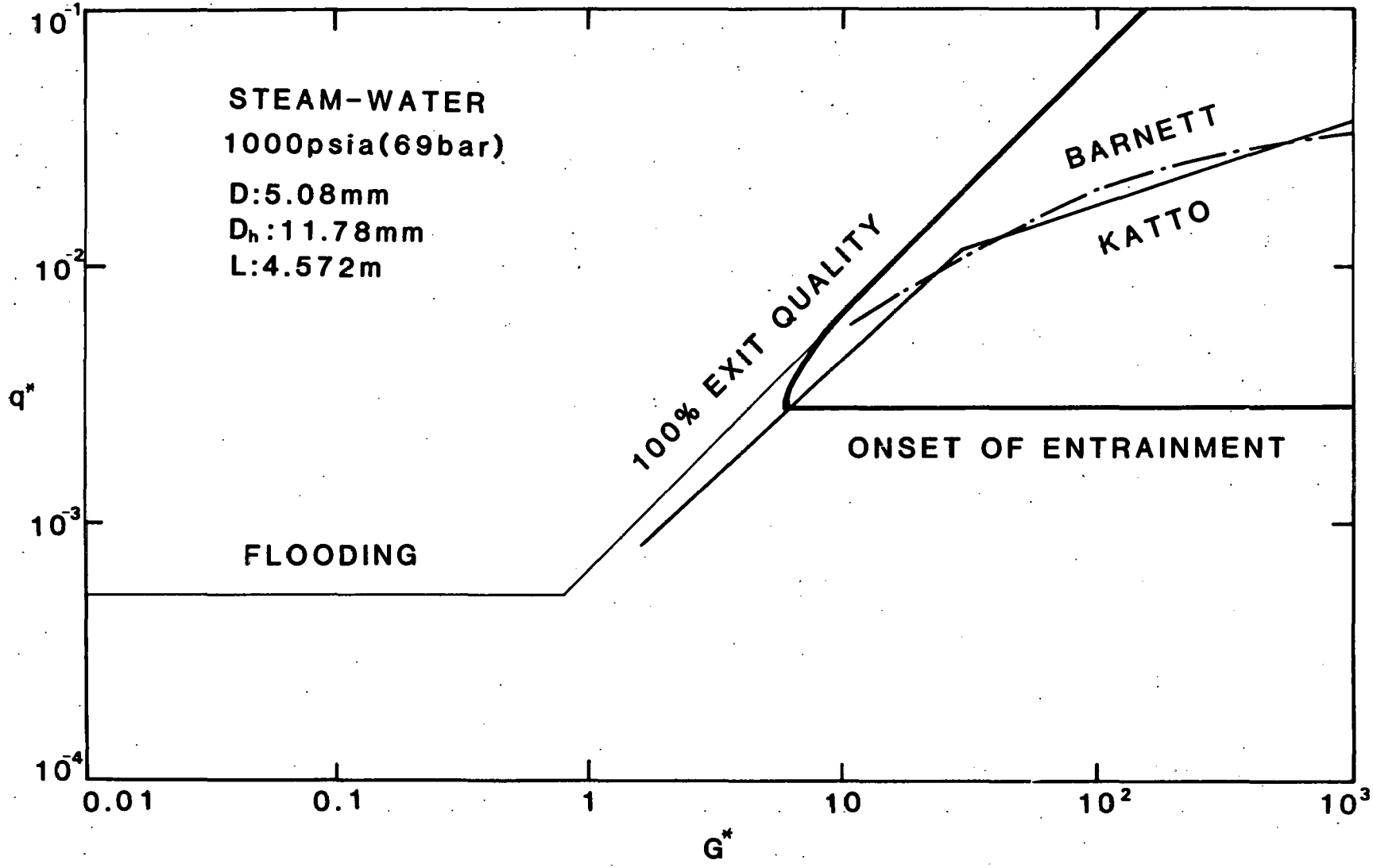

Fig. 13. Comparison of Burnout Correlations at High Pressure (69 bar) and Low Mass Velocities

REFERENCES

L. J. A. Bouré, A. E. Bergles and L. S. Tong, "Review of Two-phase Flow Instability," ASME Paper No. 71-HT-42 (1971).

2. D. B. Collins, M. Gacesa and C. B. Parsons, "Study of the Onset of Premature Heat Transfer Crisis during Hydrodynamic Instability in a Full-scale Reactor Channel," ASME Paper No. 71-HT-11 (1971).

3. P. Griffith, W. A. Schumann and A. D. Neustal, "Flooding and Burnout in Closed-end Vertical Tubes," Two-phase Fluid Flow Symposium, Paper No. 5, Institution of Mechanical Engineers, London (1962).

4. J. C. M. Leung, "Occurrence of Critical Heat Flux during Blowdown with Flow Reversal," ANL-77-4 (1977).

5. M. Ishii and K. Mishima, "Study of Two-fluid Model and Interfacial Area," NUREG/CR-1873, ANL-80-111 (1980).

6. G. G. Hewitt, H. A. Kearsey, P. M. C. Lacey and D. J. Pulling, "Burnout and Nucleation in Climbing Film Flow," Int. J. Heat Mass Trans., Vol. 8, p. 793 (1965).

7. G. F. Hewitt and N. S. Hall Taylor, "Annular Two-phase Flow," Pergamon Press, Oxford (1970).

8. D. Butterworth and G. F. Hewitt, "Two-phase Flow and Heat Transfer," Oxford University Press, Oxford (1977).

9. J. G. Collier, "Convective Boiling and Condensation," McGraw-Hill, London (1972).

10. W. J. Frea, "Two-phase Heat Transfer and Flooding in Counter Current Flow," 4th Int. Heat Trans. Conf., Paper No. B5.10, Paris (1970).

11. H. Kusuda and H. Imura, "Stability of a Liquid Film in a Counter-current Annular Two-phase Flow," Bulletin of the JSME, Vol. 17, No. 114, p. 1613 (1974).

12. Z. Nejat, "Maximum Heat Flux for Countercurrent Two-phase Flow in a Closed End Vertical Tube," 6th Int. Heat Trans. Conf., Toronto, Canada (1978).

13. J. A. Block and G. B. Wallis, "Heat Transfer and Fluid Flows Limited by Flooding," AIChE Symposium Series, No. 174, Vol. 74, p. 73 (1978).

14. P. Griffith, C. T. Avedisian and J. P. Walkush, "Counterflow Critical Heat Flux," AIChE Symposium Series, No. 174, Vol. 74, p. 149 (1978).

15. M. K. Bezrodny, S. N. Faynzilberg and YE. A. Kondrusik, "Investigation of the Maximum Heat Transfer in Annular Two-phase Thermosyphons," Heat Transfer - Soviet Research, Vol. 12, No. 1, p. 118 (1980).

16. G. B. Wallis, "Flooding Velocities for Air and Water in Vertical Tubes," UKAEA Report No. AEEW-R123 (1971).

17. M. Ishii, "One-dimensional Drift-flux Model and Constitutive Equations for Relative Motion between Phases in Various Two-phase Flow Regimes," ANL-77-47 (1977).

18. N. Zuber, "Hydrodynamic Aspects of Boiling Heat Transfer," AECU-4439 (1959).

19. S. S. Kutatelaeze, "Heat Transfer in Condensation and Boiling," AEC-tr-3770 (1959).

20. D. A. Barnard, F. R. Dell and R. A. Stinchcombe, "Dryout at Low Mass Velocities for an Upward Boiling Flow of Refrigerant-113 in a Vertical Tube," HTFS Research Symposium, AERE-R7726 (1973).

21. P. B. Whalley, P. Hutchinson and G. F. Hewitt, "The Calculation of Critical Heat Flux in Forced Convection Boiling," AERE-R7520 (1973) and 5th Int. Heat Trans. Conf., Paper B6.11, Tokyo (1974).

22. Y. Katto, "A Generalized Correlation of Critical Heat Flux for the Forced Convection Boiling in Vertical Uniformly Heated Round Tube," Int. J. Heat Mass Trans., Vol. 21, p. 1527 (1978).

23. S. S. Kutateladze, "Critical Thermal Flow for the Flow of a Wetting Liquid Containing an Underheated Core," Energetica, No. 2, p. 229 (1959).

24. M. Ishii and M. A. Grolmes, "Inception Criteria for Droplet Entrainment in Two-phase Concurrent Film Flow," AIChE J., Vol. 21, p. 308 (1975).

25. R. V. Macbeth, "Burnout Analysis. Part 4: Application of Local Conditions Hypothesis to World Data for Uniformly Heated Round Tubes and Rectangular Channels," AEEW-R267 (1963).

26. R. V. Macbeth, "The Burnout Phenomenon in Forced-convection Boiling," Advances in Chemical Engineering, Vol. 7 (1968).

27. W. H. Lowdermilk, C. D. Lanzo and B. L. Siegel, "Investigation of Boiling Burnout and Flow Stability for Water Flowing in Tubes," NACA-TN-4382 (1958).

28. P. G. Barnett, "A Correlation of Burnout Data for Uniformly Heated Annuli and Its Use for Predicting Burnout in Uniformly Heated Rod Bundles," AEEW-R463 (1966).

29. Y. Katto, "Generalized Correlations of Critical Heat Flux for the Forced Convection Boiling in Vertical Uniformly Heated Annuli," Int. J. Heat Mass Trans., Vol. 22, p. 575 (1979).

ACKNOWLEDGMENTS

We would like to express our gratitude to Elmer R. Gunchin and George Lambert who aided in the construction and operation of the experimental apparatus.

Distribution for NUREG/CR-2647 (ANL-82-6)

Internal:

E. S. Beckjord
C. E. Till
R. Avery
J. F. Marchaterre
A. J. Goldman
P. A. Lottes
L. W. Deitrich
D. H. Cho
P. B. Abramson
G. DeJarlais
I. Kataoka
W. T. Sha
Y. W. Shin
W. L. Chen
T. C. Chawla
M. Ishii (24)
G. Ridges
ANL Patent Dept.
ANL Contract File
ANL Libraries (2)
TIS Files (6)

External:

USNRC, for distribution per R2 and R4 (395)
DOE-TIC (2)
Manager, Chicago Operations Office, DOE
President, Argonne Universities Association
Reactor Analysis and Safety Division Review Committee:

W. P. Chernock, Combustion Engineering, Inc., 1000 Prospect Hill Road, Windsor, Conn. 06095
L. C. Hebel, Xerox Corp., 3333 Coyote Hill Road, Palo Alto, Calif. 94304
W. Kerr, Nuclear Engineering Dept., The University of Michigan, Ann Arbor, Mich. 48105
S. Levine, NUS Corp., 4 Research Place, Rockville, Md. 20850
S. Levy, S. Levy, Inc., 1901 S. Bascom Ave., Campbell, Calif. 95008
T. H. Pigford, Dept. of Nuclear Engineering, University of California, Berkeley, Calif. 94720
J. J. Taylor, Electric Power Research Inst., P. O. Box 10412, Palo Alto, Calif. 94303